The Institute of Space and Astronautical Science
Report SP No. 17 March 2003

An Experimental Study on the Boundary Layer Transition due to Gas Injection from Capsule-shape Body Surface

By

Tetsuya YAMADA*, Hiroyuki OGAWA*,
Satoshi NONAKA*, Yoshifumi INATANI*,
Kazuyuki NAKAKITA†, and Takashi YAMAZAKI†

(1 February 2003)

Abstract: In order to study the onset of the ablation gas-induced boundary layer transition during the reentry phase, heat flux measurement through infrared thermography has been conducted on the capsule-shape body with gas injection from the porous material surface in the shock wind tunnel. In the present simulation experiment, Reynolds number and the ratio of the gas injection mass flow rate to the main mass flow is parametrically changed as similarity law parameters taking account of those in the flight environment; not a few assumptions are applied without verification; the effect of temperature of the boundary layer and the wall etc. At the local Reynolds number of 4×10^4 and the ratio of gas injection to main flow is about 2%, the heat flux enhancement at the skirt part of the capsule model has been observed and it is considered to be an evidence of the boundary layer transition form laminar to turbulence.

1. INTRODUCTION

The Institute of Space and Astronautical Science (ISAS) has an asteroid sample return mission named MUSES-C, which is planned to be launched in 2003. In the final phase of the MUSES-C, a small capsule with asteroid sample will conduct reentry flight directly from interplanetary transfer orbit (ISAS, 2001). The capsule is exposed to severe aerodynamic heating up to 15 MW/m^2 due to its high reentry velocity. An ablator heatshield is suitable thermal protection for such reentering vehicles in high-heat flux environment. Actually a carbon phenolic ablator is adopted for the heatshield of the MUSES-C reentry capsule (Yamada, et. al., 2002).

However, it is reported that ablation gas injected from the surface can induce the boundary layer transition, which leads to enhancement of the convective heating rate. From the flight data obtained in the Pioneer-Venus mission, it was observed that the temperature is siginificantly

* Institute of Space and Astronautical Science, 3-1-1 Yoshinodai, Sagamihara, Kanagawa, JAPAN.
† National Aerospace Laboratory, 7-44-1 Jindaiji Higashimachi, Chofu, Tokyo, JAPAN.

elevated at the downstream frustum region than that at the stagnation region (Wakefield & Pitts, 1980). The heating enhancement observed in the downstream region of could be caused by the boundary layer transition indueced by ablation gas injection (Park, 1999).

Several experimental studies on laminar-to-turbulent transitions over a body withh surface mass injection have been conducted by means of porous materials. In case of the boundary layer transition, the laminar heat transfer is predicted to be increased up to the tubulent heat transfer. Kaattari (1978), calculating the heat transfer rate from calorimeter temperature versus time transients, showed the early boundary layer tronstition due to the gas injection. In the present study infrared camera has been used to measure the heat transfer rate based on the time profile of the surface temeprature, which is desirable to elminate the effect of the surface roughness of the caloriemeter on the transtion.

2. FLIGHT ENVIRONMENT FOR THE REENTRY CAPSULE

On a experiment on the boundary layer transition, it is essenstial to duplicate the Reynolds number of the flight environment in the windtunnel. The flight environment of the MUSES-C reentry capsule is shown in Fig. 1.

The Reynolds number in the boundary layer is defined based on temperature, pressure, and the velocity at outer edge of the boundary layer with the thickness as a reference length. The boundary layer Reynolds number is estimated as follows;

1) The pressure distribution on the capsule surface is estimated based on the Newtonian-theory.
2) Calculation of the velocity distribution based on the DeJarnett method (DeJarnett, 1971).
3) Calculation o the boundary layer Reynolds number based on the Cohen's correlations as for the density and the transport properties of the high temperature air (Cohen, 1960).

The Reynolds number of the boundary layer at a given altitude along the reentry trajectory is shown in Fig. 2. The boundary layer Reynolds number shows higher value at the lower altitude, and the value at the shoulder portion of the capsule-shape is higher than that in the stagnation part. The boundary layer Reynolds number at the time of the maximum heat transfer is estimated to be 1.7×10^4.

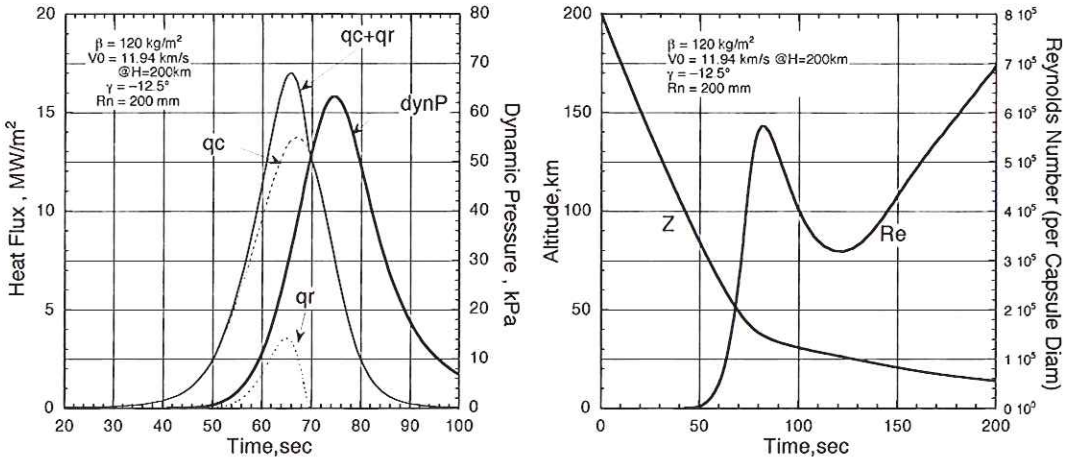

Fig. 1: Flight Environment of the MUSES-C Reetnry Capsule.

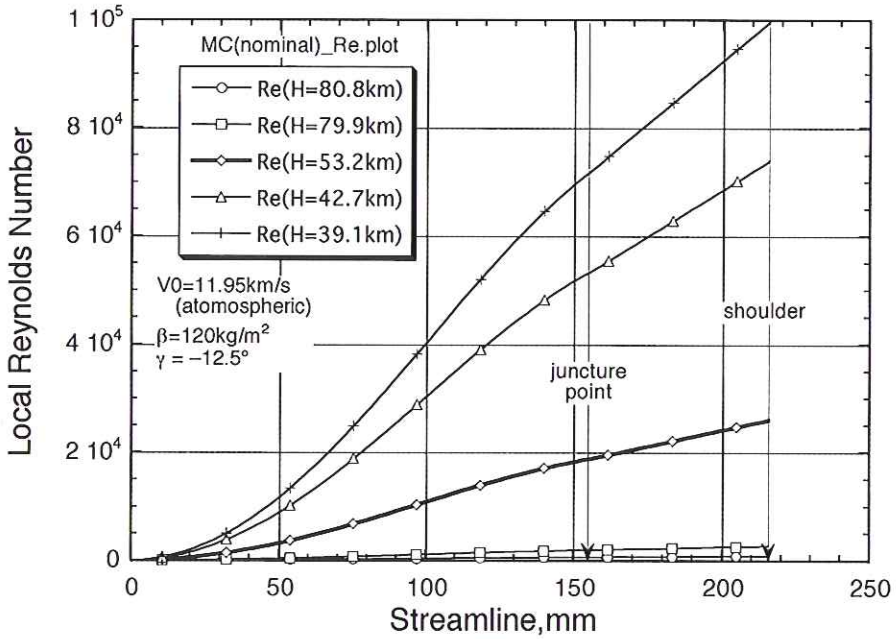

Fig. 2: Local Reynolds Number Distribution along the Capsule Surface.

Table 1: Operational Condition of the QUIC mode Shock Wind Tunnel.

	High Re	Middle Re	Low Re
High Pressure Part : P4 [MPa]	4.5	4.0	2.0
Low Pressure Part : P1 [Pa]	45	20	10
Pressure Ratio : P4/P1	100	200	200
Total Temperature [K]	940	1180	1180
Stagnation Pressure [Pa]	9100	8500	4300
Mach Number	10.45	10.3	10.3
Main Flow Velocity [m/s]	1029	1112	1173
Main Flow Mass Flow Rate [mg/cm^2/s]	958	787	411
Main Flow Reynolds Number per 1 m	2.42E6	1.55E6	0.82E6
Local Re @ Model 98 Shoulder	2.6E4	1.7E4	0.9E4
Local Re @ Model 99 Shoulder	4.3E4	3.1E4	1.7E4

3. EXPERIMENTAL APPARATUS AND PROCEDURE

3.1 Shock Wind Tunnel

The middle-size shock wind tunnel at NAL (National Aerospace Laboratory) operates in two modes; one is normal shock wind tunnel operation, and the other is QUIC (Quasi Isentropic Compression) mode (Soga, Inoue, et. al., 1992). The special feature of the QUIC mode is as follows; 1) It can operate with long duration up to 40 ms because it does not use double diaphragms. 2) It is quasi-isentropic compression due to relatively weak shock wave properga-

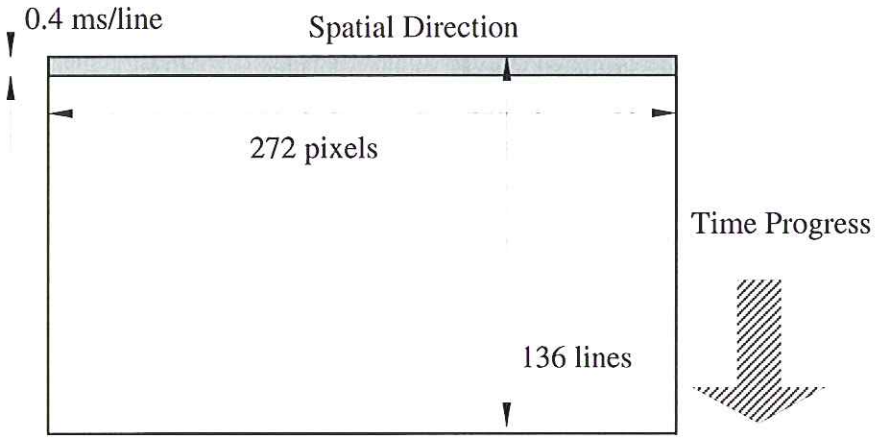

Fig. 3: IR Thermography Data Acquisition

tion. In order to obtain higher Reynolds number, the operation condition with the higher total pressure and the lower total temperature is required. Taking account of the operation envelope of the shock tunnel in QUIC mode, the highest Reynolds number is accomplished with high P4 (pressure at the high pressure storage tank) and high P4 to P1 (pressure at the low pressure tube) as shown in Table 1. It is clear that the shock tunnel in QUIC mode is ideal for the simulation of the Reynolds number of the flight environment of the reentering capsule body.

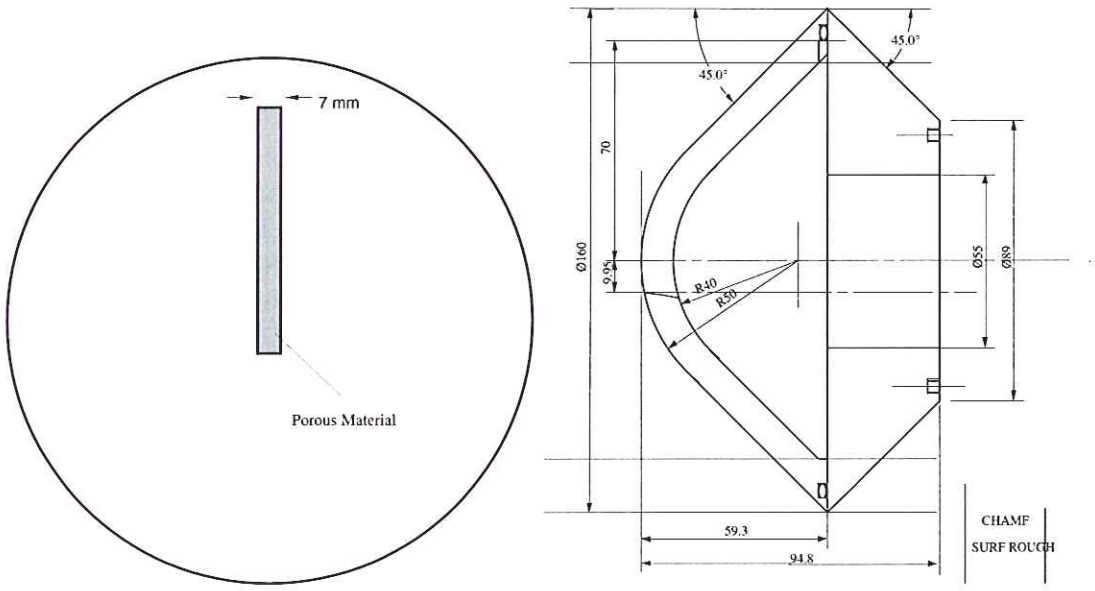

Fig. 4: Cross Sectional View of the Test Model (99B).

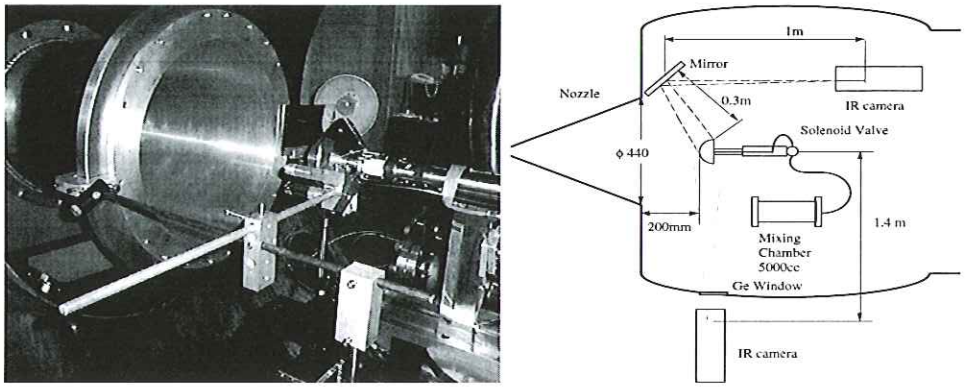

Fig. 5: Test Model and Experimental Setup.

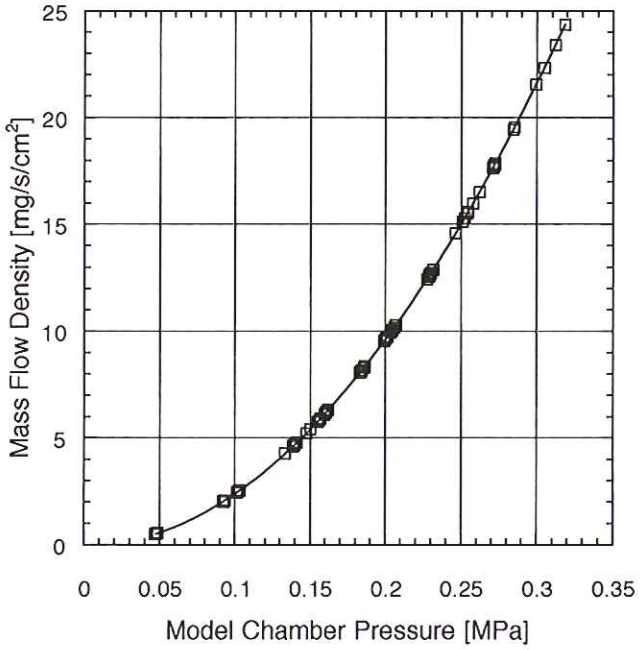

Fig. 6: Injection Mass Flow Rate vs. Model Chamber Pressure Characteristics.

3.2 High Speed Heat Flux Measurement by Infrared Thermography

In general the boundary layer transition from laminar to turbulence is considered to lead to the enhancement of the heat flux on the surface. We will obtain some clue as for the boundary layer transition by measuring the heat flux distribution. Inoue et. al. established the infrared (IR) thermography technique by means of the infrared camera in the hypersonic wind tunnel (Inoue, Yoshizawa, et. al). The duration of the hypersonic wind tunnel with duration of 30 sec enables the thermography system to obtain 2 dimensional temperature distribution images. The thermography technique needs to be improved so that data acquisition can be completed within several tens of mili-seconds ms within the duration of shock wind tunnel in QUIC

mode. In the present study, the IR thermography system was expanded so that it can scan 1-dimensional temperature profile in 0.4 ms; The 2-dimensional image must be given up due to the CPU speed of the data handling unit. As shown in Fig. 3, the scanning of the 1 line takes 0.4 ms (Frequency : 2.5 kHz), and 136 lines in the time-progress-wise direction are integrated to 1 frame. The resolution of the temperature measurement is 0.08° C (12 bit data for 100°C). The heat flux is deduced from the time profile of the surface temperature by means of Shultz and Jones Method (Shultz and Jones 1973) expressed as

$$\dot{q} = \sqrt{\frac{\rho c k}{\pi}} \left[\frac{T(t)}{\sqrt{t}} + \frac{1}{2} \int_0^t \frac{T(t) - T(\tau)}{(t-\tau)^{3/2}} d\tau \right] \tag{1}$$

where ρ : density, c : specific heat, k : heat conductivity, τ : measurement time, and T(t) : temperature at time t. Here the aerodynamic heating rate is assumed to be constant during the measurement time τ.

The above equation is valid under the assumption of infinite slab approximation that means the thickness of the slab has no effect on the conduction of the heat. The thickness of the material must satisfy the next relation between thermal diffusivity (α) and the duration (t) of the aerodynamic heating expressed as

$$thickness > 4\sqrt{\alpha \cdot t} \tag{2}$$

The thermal diffusivity of the material used for the experiment needs to be low enough that the thermal penetration depth of the material due to the aerodynamic heating is small in comparison with the material geometrical thickness.

3.3 Test Model with Gas Injection

The ablation gas from the surface of the reentering body is simulated by the gas injection from the surface of the porous material of the test body under the assumption as follows; 1) The air in the room temperature is used for the injection gas. 2) The effect of the injected gas temperature and the wall temperature is negligible.

Because the diameter of the carbon fiber ranges 10 to 20 μm in case of the carbon phenolic ablator such as used of the MUSES-C reentry capsule, the gas should be injected from the holes with the diameter of the same order with the fiber. Thus the porous ceramics made of Aluminum Borate ($9Al_2O_3 \cdot 2B_2O_3$) has been used for the test model, of which mechanical and thermal properties are summerized in Table 2 (Iizuka, 1998).

Table 2: Porous Aluminum Borate Properties.

Chemical Composition	Aluminum Borate ($9Al_2O_3 \cdot 2B_2O_3$)
Porosity	72% (normally 80-20%)
Allowable Bending Stress	10-200 [MPa]
Heat Conductivity ($V_f = 25\%$)	(0.528 W/mK (600 deg C)
Thermal Expansion Coeff ($V_f = 25\%$)	4.8E-6 [/deg C]
Maximum Temperature	1300 [deg C]

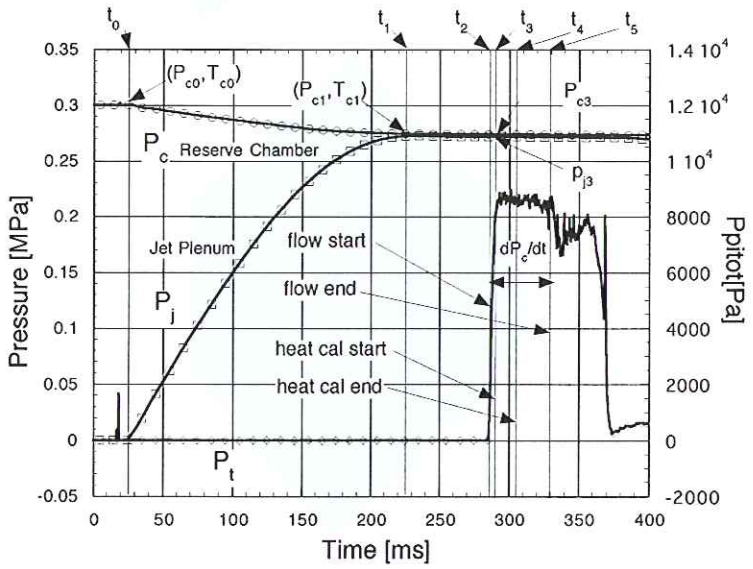

Fig. 7: Typical Time Profile of the Wind Tunnel Operation.

A cross sectional view of the test model used for the present study is shown in Fig. 4. Because the total gas injection mass flow needs to be within the gas supply ability and the evacuation ability of the wind tunnel, the porous material is installed only in the strip region on the surface with the width of 7 mm.

As a similarity law, the ratio of the gas injection mass flow rate to the main mass flow (ρ u : density multiplied by flow velocity) is parametrically changed taking account of those in the flight environment.

Figure 5 shows the experimental apparatus arrangement in the shock wind tunnel facility. The mass flow rate of the injection gas is estimated based on the pressure decay profile of the gas-supply mixing chamber installed upstream of the test model.

Gas Injection

The mass flow rate of the gas injection was correlated to the model surface pressure (Ps) and the model chamber pressure (Pc) as follows;

$$\dot{m} = C\left(P_{chamber}^2 - P_{surface}^2\right) \tag{3}$$

The coefficient C had been measured in advance to the experiment. As shown in the shock tunnel operation condition, the surface impact pressure on the model is about 10 kPa while the model chamber pressure ranges 100 to 500 kPa. Because the mass flow rate is proportional to the difference of their square, the gas injection rate distribution due to the impact pressure distribution is trivial at most 1%. Figure 6 shows the mass flow density vs. the model chamber pressure characteristics.

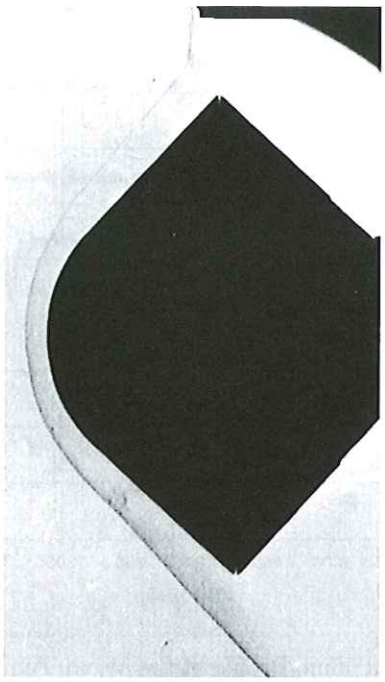

Fig. 8: A Schlieren Photograph in case of no gas injection.

4. EXPERIMENTAL RESULT AND DISCUSSION

4.1 Experiment Sequence

Figure 7 shows a typical time profile of the wind tunnel operation together with the pressure of gas-supply mixing chamber. After appropriate time delay of the valve-open signal for the high-pressure tank (P4), the solenoid-valve downstream of the injection chamber is opened and the gas begins to blow out from the test model. Within about 100 ms, the main flow is build up as recognized from the pressure at the test section. Fig. 8 show a typical Schlieren photograph of the test piece without gas injection. Any differences in the Schlieren photos with / without gas injection are not clearly observed, perhaps because the density gradient is too small to be detected in the shock wind tunnel.

4.2 Blockin Effect of Stagnation Point Heat Transfer

The effect of the mass addition on the stagnation point heating (Marvin, 1967) is generally well predicted for laminar flow by

$$\psi = \frac{\dot{q}_{stagnation}}{\dot{q}_{0,stagnation}} = 1 - 0.72B + 0.13B^2 \tag{4}$$

$$B = \frac{\dot{m}\Delta H}{\dot{q}_{0,stagnation}} \tag{5}$$

where $\dot{m}$ is mass addition rate and ΔH is the heat transfer driving potential defined as the difference between the wall enthalpy and the stagnation enthalpy. The term ψ is the ratio of the heat transfer $\dot{q}_{stagnation}$ at the presence of mass addition with respect to the heat transfer

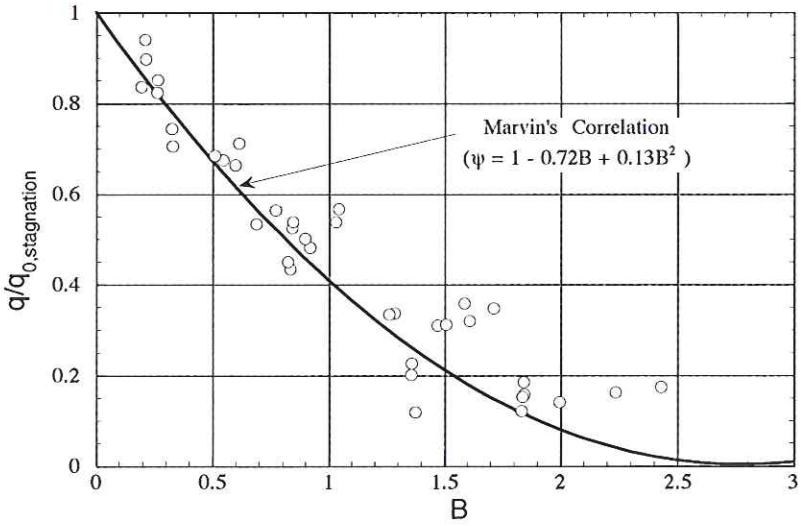

Fig. 9: Correlation of Convective Heating Rate Ratio ψ with Mass Addition Paramter B.

$\dot{q}_{0,stagnation}$ with no mass addition. The independent variable B is the blowing parameter. ψ of all data have been plotted versus B together with Marvin's correlation as shown in Fig. 9. In the present experiment conduected in the shock windtunnel, the blowing parameter ranges 0 to 2.5 and then ψ the ratio of the heat transfer ranging 1 to 0.1 is well correlated to Marvin's correlation though not a small dispersions are seen in high B region.

4.3 Heat Flux Distribution and the Effect of the Gas Injection

The surface heat flux distributions normalized by the stagnation value are shown in Fig. 10 to Fig. 12 through with the parameter of the ratio of injection mass flow rate (m) to the main mass flow rate (M).

When the gas injection rate equals to zero, the heat flux distribution is almost identical to Lee's distribution. The qualitative features in case of gas injection are as follows;
1) The heat flux distributions are uniformly decreased with increased m/M ratio regardless of the Reynolds number.
2) The heat flux distributions in the high and middle Reynolds number exhibit unique aspect that the heat flux downstream of the model juncture point (frustum part) onsets increase beyond a certain m/M ratio. For example, the heat flux in the high-Reynolds condition start to increase at and beyond m/M is 1.81%. Moreover the heat flux at the frustum part is higher than the value at the low m/M ratio such as 1.1% and 0.65%. Actually it is observed that the heat flux is below zero in a some portions, this is considered to be caused by the cold gas injection.

This phenomenon that the heat transfer increase at the frustum region is considered to be the heat flux enhancement and it might be reasonable that this is an evidence of the boundary layer transition due to ablation-simulated gas injection.

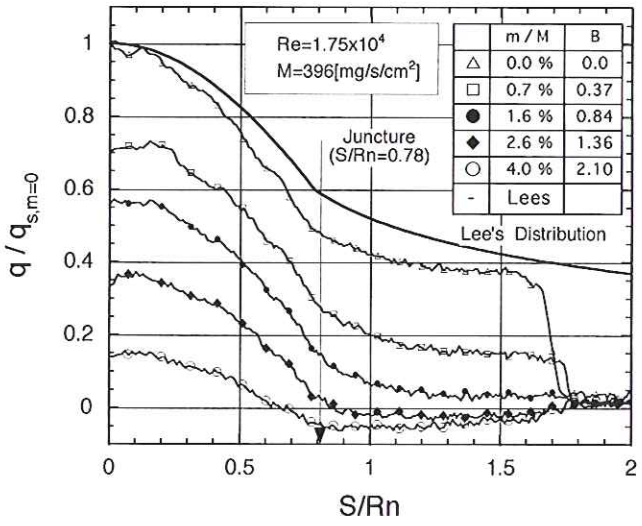

Fig. 10: Heat Flux Distribution along the Surface (Low Re).

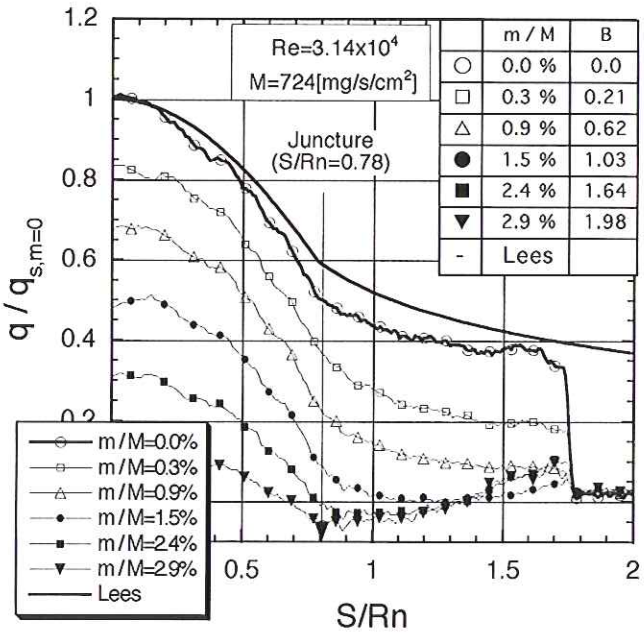

Fig. 11: Heat Flux Distribution along the Surface (Middle Re).

4.4 Boundary Layer Transition along the Reentry Trajectory

On the basis of the criterion described above, the onsets of the boundary layer transition are mapped along the reentry trajectory of the MUSES-C reentry capsule as shown in Fig. 13. The vertical axis denotes the m/M ratio (ablation mass flow rate to main mass flow) based on the

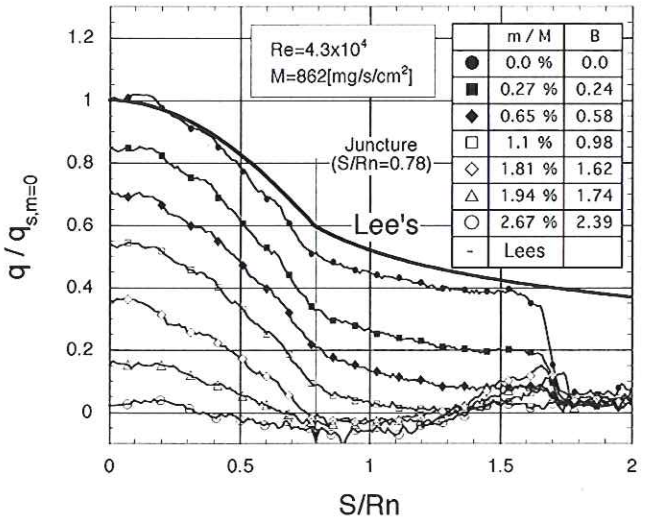

Fig. 12: Heat Flux Distribution along the Surface (High Re).

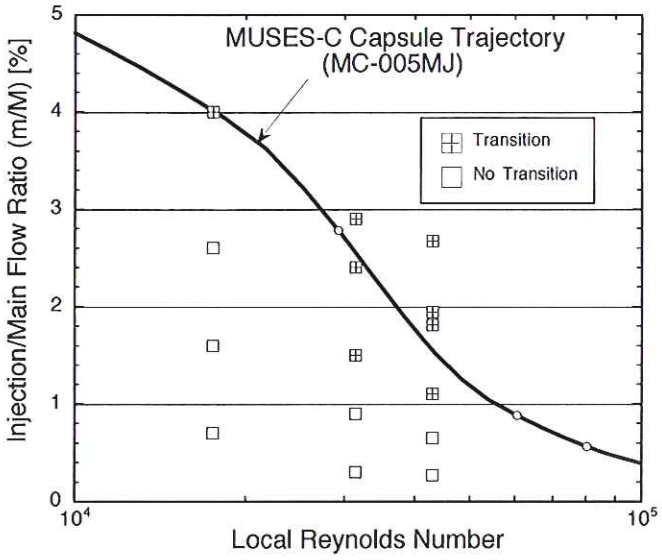

Fig. 13: Onset Mapping of the Boundary Layer Transition aalong the MUSES-C Reentry Trajectory (MC-005MJ).

ablator analysis along the reentry trajectory. Judging from this figure, we might conclude that the possibility of the onset of the boundary layer transition and resulting heat flux enhancement is small during the reentry.

5. CONCLUSION

In order to study the onset of the ablation gas- induced boundary layer transition during the reentry phase, heat flux measurement has been conducted by means of gas injection from the test model made of porous material in the shock wind tunnel through infrared thermography. In the present simulation experiment, Reynolds number and the ratio of the gas injection mass flow rate to the main mass flow is parametrically changed as only similarity law parameters taking account of those in the flight environment; not a few assumptions are applied without verification; the effect of temperature of the boundary layer and the wall etc. Although authors recognizing these insufficiency would like to conclude as follows; At the local Reynolds number of 4×10^4 and the ratio of gas injection to main flow is about 2%, the heat flux enhancement at the frustum part of the capsule model has been observed and it is considered to be an evidence of the boundary layer transition form laminar to turbulence.

REFERENCES

N. B. Cohen, "Correlation Formula and Tables of Density and Some Transport Properties of Equilibrium Dissociating Air for Use in Solutions of the Boundary Layer Equation", NASA TN D-194, 1960.

Iizuka, "Porous Aluminum Borate', Nichias Co. Product Catalogue", 1998.

Iizuka, T., Narita, T., Sakane, T., "Fabrication and Properties of Porous Ceramics with a Skelton Structure of Aluminum Borate Whiskers", J. Ceramic Soc. Japan, 106 [3], p. 327, 1998.

Inoue, Y., Yoshizawa, A., Koyama, T., Tsuda, S., Yamamoto, et. al., "Quantitative Measurement of the Aerodynamic Heat Transfer in the Hypersonic Flow by Infrared Thermography", p.105, Proc. Symposium on Astrodynamics, 1996.

Kaattari, G. E., 1978, Effects of Mass Additon on Blunt-Body Boundary-Layer Transition and Heat Transfer, NASA TP-1139.

F. R. DeJarnette, "Calculation of Inviscid Surface Streamline and Heat Transfer on Shuttle-type Configuration", NASA CR-111921, 1971.

Marvin, Jeseph G. and Pope, Ronald B., "Laminar Convective Heating and Ablation in the Mars Atmosphere", AIAA Journal, vol.5, no.2, 1967.

Park Chul, "Injection Induced Turbulence in Stagnation Point Boundary Layers", AIAA J. 22 (1984) p.219.

Park Chul, "Ablation of Galileo Probe Heat-Shield Models in a Ballistic Range", AIAA J. 23, (1985), p.301.

Park Chul, "Heatshielding Problems of Planetary Entry, A Review", AIAA Paper 99-3415.

Soga, K., Yamazaki, T., and Shirouzu, M., "NAL middle-size shock wind tunnel", NAL-A19920045, 1992.

D.L. Schultz and T.V. Jones, "Heat-transfer Measurements in Short Duration Hypersonic Facilities", AGARDO graph No.165, p.149, 1973.

Wakefield R. M. and Pitts, W. C., "Analysis of the Heatshield Experiment on the Pioneer-Venus Entry Probes", AIAA 80-1494.

Yamada, T., Inatani, Y., Honda, M., Hirai, K., "Development of Thermal Protection System of the MUSES-C/DASH Reentry Capsules", Acta Astronautica Vol.51, No.1-9, pp.63-72,2002.